Effect of electric load and dual atmosphere on the properties of an alkali containing diopside-based glass sealant for solid oxide cells

A.G. Sabato[1]*, A. Rost[2], J. Schilm[2], M. Kusnezoff[2], M. Salvo[1], A. Chrysanthou[3], F. Smeacetto[4]

[1] Department of Applied Science and Technology, DISAT, Politecnico di Torino, Corso Ducadegli Abruzzi 24, 10129 Torino, Italy

[2]Fraunhofer Institute of Ceramic Technologies and Systems, Winterbergstraße 28, 01277, Dresden, Germany

[3] School of Engineering and Technology, University of Hertfordshire, Hatfield AL10 9AB, UK

[4]Department of Energy, DENERG, Politecnico di Torino, Corso Duca degli Abruzzi 24, 10129 Torino, Italy

* corresponding author, e-mail antonio.sabato@polito.it, phone +39 011 0904756

Abstract

A new alkali-containing diopside based glass-ceramic sealant for solid oxide cells was synthesized, characterized and tested. The composition was designed to match the coefficient of thermal expansion (CTE) of Crofer22APU interconnect. The sealant has a glass transition temperature of 600°C, a crystallization peak temperature of 850°C and a maximum shrinkage temperature of 700°C, thus suggesting effective densification prior to crystallization. The CTE of the glass-ceramic is 11.5 10^{-6} K^{-1}, a value which is compatible with the CTE for Crofer22APU stainless steel. Crofer22APU/glass-ceramic/Crofer22APU joined samples were tested in simulated real-life operating conditions at 800°C in dual atmosphere under an applied voltage, monitoring the electrical resistivity. The effect of two different applied voltages (0.7V and 1.3V) was evaluated. A voltage of 1.3V led to a rapid decrease in the electrical resistivity during the test;such a drop was due to the formation of Cr_2O_3 “bridges” that connected the two Crofer22APU plates separated by the sealant. There was no decrease in the resistivity when a voltage of 0.7V was applied.

Instead,resistivity value remained stable at around 10^5 Ω cm for the 100h test duration. The degradation mechanisms, due to both the alkali content and the applied voltage, are investigated and discussed.

Introduction

In recent years much effort by the scientific community has focused on solid oxide cell (SOC) technology [1-5] which is attractive due to a high achievable efficiency [6,7]. A further advantage is the possibility to design reversible devices that can act both as electrolyzers (solid oxide electrolysis cells SOEC) as well as electrical power generators (solid oxide fuel cells SOFC) [8,9]. In both configurations, the operating conditions are rather extreme [5,7,10,11], involving reducing and oxidizing atmospheres, high operating temperatures (750-850°C) and long operating periods (at least 40,000h). The design of devices for use under these conditions involves the selection of such materials as to minimise degradation rates for the entire lifecycle of the SOC apparatus. In both operating modes (electrolyzer or fuel cell mode), it is necessary to connect many cells in series in a stack [6,10,11]. This way, it is possible to reach usable output power in the case of SOFC or feasible hydrogen production amounts in the caseof SOEC.

A very important component in the planar stack design is the sealant; its function is crucial in order to guarantee the correct operation of the SOC stack for its complete service life [6,11-14]. The sealant is exposed to both oxidizing and reducing environments at elevated temperatures and its main role is to prevent gas mixing. Therefore, it must maintain gas tightness and integrity during the entire life of the device and needs to be thermo-mechanically compatible with the sealed metallic and ceramic components. The sealant must also be chemically stable at the operating conditions in order to avoid detrimental reactions with the joined materials and with the atmospheres to which it is exposed [6,11-

14]. Furthermore, since the sealant must operate under an applied electrical voltage, it requires high electrical resistivity in order to avoid current shunting and development of electrochemical reactions [13-18].

Among the different classes of materials investigated during recent decades, glass-ceramics seem to be the most promising, owing to their high chemical stability under the operating conditions. In addition, an accurate design of their composition allows the tailoring of their properties (e.g. coefficient of thermal expansion, electrical resistivity, viscosity and characteristic temperatures). Diopside ($CaMgSi_2O_6$) based glass-ceramics have been identified as potential materials for SOC sealing application [14,19-22] owing to the high chemical stability of diopside and its coefficient of thermal expansion [23]. The crystallization of this phase could help tailor the overall properties of the glass-ceramic sealant to satisfy the requirementsfor application on planar SOC stacks (i.e. improving its mechanical and thermomechanical properties).

The introduction of alkali oxides in the glass as network modifiers represents an effective strategy for lowering the viscosity of the system, the glass transition temperature (T_g) and the softening temperature (T_s) [12,13,24]. The joining process is carried out at a temperature higher than the softening point [25-28] and the viscous behaviour of the material allows high densification (when starting from the powder form) leading to more effective wetting of the components to be sealed. The introduction of alkali oxides also increases the CTE of the glass-matrix [12,13,24] and can therefore play a significant role in the tailoring of the thermo-mechanical properties of the glass-ceramics, making them compatible with the sealed components.

However, the behaviour of alkalis in typical SOC working conditions has been debated and it is rather controversial. Many studies [12,14,29-31] have reported the detrimental effects of these elements that can react with the Cr contained in the ferritic stainless steels,

typically used as interconnect materials (like Crofer22APU or AISI441), with the consequent formation of volatile chromates. This is crucial, since in many planar stack designs the sealants need to be placedbetween the frames and the interconnects which are both made from ferritic stainless steel. The formation of chromates (such as Na_2CrO_4, K_2CrO_4, $BaCrO_4$ or $SrCrO_4$) is due to the reaction between the sealant and the interconnect and may compromise the integrity of the joint or lead to cathode poisoning (in case of volatile chromates) [30,32]. The correct order of events involved in degradation mechanisms and the effect of different operating conditions (i.e. composition of the atmospheres, pre-oxidation of steels, applied voltages) is still unclear. Detrimental reactions would be expected to take place at the interface between the interconnects and the alkali-containing sealants. However, Ogasaswara et al. [30] pointed out that the reactions between Cr and alkalis occurs mainly between gaseous species at the air side. In their study they supposed that the reaction occurred between Cr in the oxide scale of the interconnect and gaseous KNO_3 and $NaNO_3$, formed at the air side of an alkali-containing sealant. However KNO_3 and $NaNO_3$ are not stable at typical operating temperatures for SOFC and decompose. Therefore we consider this reaction path as rather unlikely. Another possible explanation could be reaction between gaseous Cr-containing species, such as $CrO_2(OH)_{2(g)}$ and alkali oxides contained in the sealant.

In spite of this, many alkali-containing glassy systems have been successfully tested in the past [20,22,25,33-39]. Some of them were also thesubject of patents [40-42] or are commercially available (e.g.SCN-1 from SEM-COM, Toledo, OH). These systems, when submitted to relevant conditions (i.e. dual atm.), in contact with Crofer22APU or AISI441 stainless steels, did not show any formation of volatile species and guaranteed gas tightness even after long term exposure (more than 500h). For example, Chou et al. [33-35] successfully tested commercial sealant SCN-1, containing Na and K, for sealing

AISI441 stainless steel in different relevant conditions by conducting thermal cycling, dual atmosphere and long term aging (at least 500h at 700°C, 750°C and 800°C). The long term (up to 10,000h at 800°C) compatibility between alkali containing glasses and 8% yttria-stabilised zirconia (8YSZ), which is the electrolyte material, was evaluated by Shyam et al. [43]. No detrimental reaction between the alkali metal oxide and 8YSZ was found in this study.

In our previous studies on alkali-containing diopside-based glass-ceramics sealants [20,22,44], it has been found that the strong heterogeneous nucleation of diopside, at the interface with the interconnect material may prevent detrimental reactions between the alkalis in the glassy phase and the Cr in the steel/oxide scale. However, to the authors best knowledge there are no papers focused on the testing of alkali-containing diopside-based sealants under relevant conditions, i.e. dual atmosphere with applied voltage.

The present authors consider the nature of the glass-ceramics as an opportunity to encourage the crystalline phase (that does not contain sodium) to heterogeneously crystallise at the surface of the interconnect; such an approach will potentially lead to shielding of the chromium oxide from sodium and prevent chromate formation at the interface. Moreover, the exact mechanism of the degradation of SOC stack performances, due to the presence of alkali oxides in the glass-ceramic sealants, is not completely clear and fully understood. To the authors best knowledge, there is a lack of studies focusing specifically on this aspect.

This paper focuses on the design, characterization and testing of a new Na-containing diopside-based glass-ceramic composition. Crofer22APU/glass-ceramic/Crofer22APU joined samples were tested for 100h in conditions similar to performance conditions for SOFCs: 800°C in dual atmosphere with the application of a DC electrical voltage. Despite a period of 100h is significantly shorter than the expected operating life for a SOFC stack

(i.e. 40,000h), the obtained results can be considered as predictive of the behaviour of these systems under relevant conditions for longer periods, thus providing insights for the use of Na-containing sealants when high voltage is applied to the stack. Rost et al. have published studies on the degradation behavior of other types of SOFC-sealing glasses by using this apparatus [45]. They have shown that sealing glasses containing reactive components (i.e. ZnO) tend to react stronger with the steel interface by redox-reactions what in turn leads to a strongly decreased resistance within a limited testing period up to max. 300h. The glass-ceramic studied here was obtained by modifying a previous glass composition that had successfully survived periods longer than 1000h in a dual atmosphere or in air at 800°C, without the application of electrical voltage [22,44]. The changes in the compositions were tailored in order to increase the content of diopside in the glass-ceramic, which in turn led to a CTE value more suitable for its thermo-mechanical compatibility with Crofer22APU. The role of Na in the degradation of the electrical resistivity in these conditions is reviewed and discussed and the study attempts to further investigate the involved mechanisms, paying particular attention to the effect of different applied voltages. A similar approach was previously adopted by Rost et al. on Ba-containing glass-ceramics [26,45,46].

Experimental

The investigated glass-ceramic was designed using the SciGlass® database (Science Serve GmbH, SciGlass 6.6 software, Newton, MA, USA) and was labelled V10. It was produced by conventional melting and casting, starting with high purity grade oxide or carbonate precursors. The V10 sealant has the following composition in wt%: SiO_2 49.3%, Na_2O 9.3%, Al_2O_3 8.3%, B_2O_3 5.8%, MgO 13%, CaO 14.3%. For MgO, CaO and Na_2O,the respective carbonates were used as starting powders (Sigma Aldrich, purity higher than

99.9%), while for the B_2O_3, H_3BO_3 (Sigma Aldrich, purity higher than 99.9%) was used. The parent glass composition was designed on the basis of the results obtained for the previous system labelled V9 [22], with the purpose to increase the content of CaO and thus extend the amount of diopside in the glass-ceramic in order to increase the CTE to a value closer to that for Crofer22APU.

The raw powders were mixed in the right proportions before melting, taking into account the decomposition of carbonates and acids used as precursors in order to derive an accurate final composition as reported above. The glass was produced in a Pt-Rh crucible at 1600°C with a heating rate of 10°C min^{-1} and cast as frit in deionized water at room temperature. The frit was subsequently milled in a planetary ball mill (Fritsch, Pulverisette 5, Mark Einersheim, Germany) in agata crucibles for 12h. The obtained powders were characterized by means of differential thermal analysis (DTA) and heating stage microscopy (HSM) in order to study their sinter-crystallization behaviour. DTA (Netzsch, DTA 404 PC, Eos, Selb, Germany) was performed using 100mg of the glass powder against 100mg of Al_2O_3 (Alfa Aesar, purity higher than 99,99%) that was used as the reference material at a heating ramp of 5°C/min from room temperature to 1200°C. The same heating program was used for Hot Stage Microscopy (HSM; Hesse Instruments, Osterode, Germany,). A cylindrical powder compact, 2 mm in diameter and 2 – 3 mm in height was placed on a Crofer22APU steel substrate that had been pre-oxidised at 900°C for 10h in air. In this configuration, the sintering and subsequent wetting properties of glass was investigated on the interconnect material, used for SOC-stacks. On the basis of the results of thermal characterization, the joining thermal treatment was chosen to be at 850°C. for 1h in air.

The crystalline phases, formed in the glass-ceramic, were studied by X-ray diffraction (XRD). The XRD measurements were carried out in the diffractometer D8 Advance (Bruker AXS,

Karlsruhe, Germany) with CuK_α radiation and with a LynxEye position-sensitive detector (PSD) and a nickel filter located in the primary beam. The analyses for the glass-ceramic were carried out after the joining treatment at 850°C for 1h, as well as after two different aging periods at 800°C for 100h and 300h. The powders for the analyses were obtained by crushing the pellets following the thermal treatments. Qualitative analyses were carried out using DIFFRAC.EVA (Bruker AXS) and quantitative analyses were performed using Rietveld refinement with pure crystalline Si as the internal standard and Topas V5 (Bruker AXS) with structural data from ICSD.

The V10 dilatometric behaviour was investigated by dilatometry (DIL,Netzsch, DIL 402 PC/4). The measurements were carried out using a heating rate of 5°C/min with an automating softening point detection. The CTE of each sample was measured between 200-500°C. The samples that were investigated by DIL were the glass, that was cast on a brass plate, and the glass-ceramic pellets. Three different glass-ceramic pellets were analysed; pellets after joining and after aging for 100h and 300h at 800°C.

The V10 sealant was tested in contact with pre-oxidised Crofer22APU stainless steel that was used as the interconnect material. The pre-oxidation was carried out at 900°C for 10h, for all the joined samples. In order to investigate the compatibility between these materials after the joining process, a Crofer22APU/V10/Crofer22APU sandwich sample was processed by depositing the glass onto Crofer22APU using screen-printing (EKRA Microtronic 2; Eduard Kraft GmbH, Kirchheim, Germany). For screen printing, a printable paste was produced out of the glass powder and applied on the top and bottom Crofer22APU-substrate. With a manually layered paste applied before the joining process, joining heights of about 250 µm were reached. After the aging process, the sampleswere embedded in resin and cross-sectioned with a diamond wire saw (WELL 6234, well Diamantdrahtsagen GmbH; Mannheim, Germany). These were ground and polished

according to an internal procedure used at the IKTS, developed for combinations of tough and brittle materials. For electron microscopy, the cross-sections were coated with graphite for morphological and chemical analyses by means of FESEM/EDS (Zeiss Ultra 55, Oberkochen, Germany).

The V10 glass-ceramic, coupled with pre-oxidised Crofer22APU was also tested under simulated operating conditions of a SOFC stack. Crofer22APU/V10/Crofer22APU joined samples were exposed to a dual atmosphere environment: oxidizing on one side and reducing on the other, with the application of a DC electrical voltage. A mixture of 10vol% H_2, 7vol% CO_2, 80vol% N_2, 3vol% H_2O was used as the simulated fuel atmosphere, while the oxidizing one was static air. Details of experimental apparatus for the dual atmosphere test in presence of applied voltage can be found in [45]. These samples were tested for 100h, after the joining process, at 800°C, monitoring the electrical resistivity of the system. For the accurate evaluation of the resistivity, it is very important to know the exact dimensions of the joint and therefore screen-printing wasused for the deposition of the sealant, as described above for the as-joined sample. The application of electrical potential and the measurement of the resistivity were carried out by welding Pt wires to the steel plates before joining. Two different electrical voltage values were used: 0.7V and 1.3V for comparison. Power supply and detection of the current, for calculating the resistivity was conducted by a HAMEG HM7044 four fold power supply, respective four precision multimeters HM8112-3 (HAMEG Instruments GmbH, Mainhausen, Germany). Post-mortem morphological SEM/EDS analyses were performed on cross-sections of these samples after the test. The investigations were carried out in the middle part of the joint as well as at the three-phase boundary region at the air side, i.e. Crofer22APU/sealant/air.

For comparison, the electrical resistivity was also measured on the glass-ceramic that was not in contact with the Crofer22APU; for this purpose, a cylindrical pellet was prepared and

treated at 850°C for 1h. Pt wires were adhered to the glass-ceramic using a gold-based paste and the electrical resistivity was measured for 100h at 800°C in air with a constant applied voltage of 1.3V.

The gas tightness of the joined samples after the dual atmosphere tests was assessed by He-leakage rate measurement with a Phoenix L300 (Leybold GmbH, Colone, Germany) equipped with a suitable sample holder.

Results and Discussion

In order to compare the sintering and crystallization behaviour of the glass system, DTA and HSM analyses were carried out. Fig. 1a compares the experimental data obtained from DTA and HSM analyses.

The V10 glass (in the form of powder) showed a glass transition temperature (T_g) of 600°C and a crystallization peak temperature (T_p) of 850°C. It is apparent from the results of the correlational analysis that the crystallization peak was at a temperature higher than the maximum shrinkage temperature (T_{ms}), as detected by HSM. This suggests that no overlap between the two phenomena occurred under these conditions, indicating that the crystallization of the glass does not hinder the sintering process by viscous flow nor the densification of the material. The HSM software also detected the first shrinkage temperature (T_{fs}) and the melting temperature (T_m). The pictures of the sample corresponding to the characteristic temperatures detected by HSM are reported in Fig. 1b. It is noticeable that the temperatures of sphere (T_{sp}) and half-sphere (T_{hs}) are missing from these data. This means that the instrument did not detect these shapes. This was likely to be due to the fact that the glass that was in contact with the pre-oxidised Crofer22APU sample undergoes strong crystallization at the interface (confirmed by SEM analyses

shown in Fig. 1c); this provides the HSM pellet with a more rigid structure and thus does not allow the detection of shapes corresponding to lower viscosity values.

The thermo-mechanical compatibility between the V10 and pre-oxidised Crofer22APU was confirmed by morphological SEM analyses. In Fig. 1c, the sealant appears to be well-bonded to the steel counterpart without the formation of cracks or delamination at the interface. The interface appears to be intact without evidence of adverse reactions and no formation of volatile products like sodium chromates. This is due to the formation of an almost continuous layer of diopside crystals, confirming the heterogeneous interface crystallization suggested by HSM analyses, that shielded the chromium oxide in the steel to prevent any interaction with Na in the glassy part of the sealant.

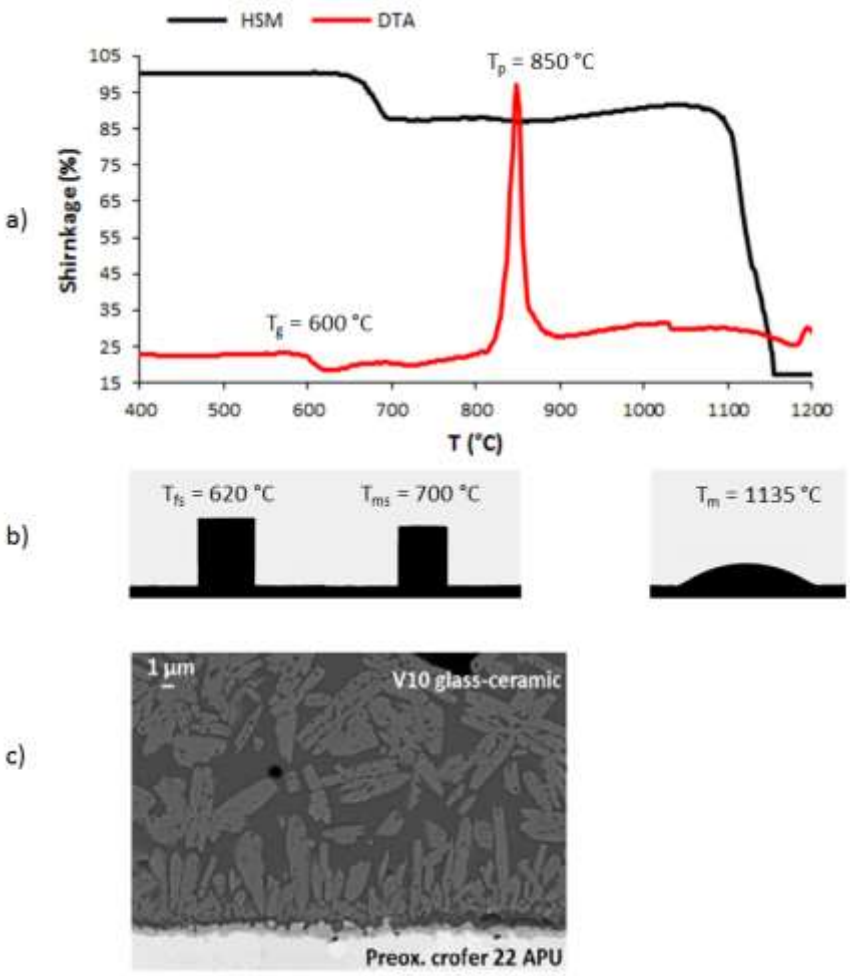

Figure 1: Superimposition of HSM and DTA results for V10 glass powders (a), shapes of the samples recorded by HSM corresponding to characteristic temperatures T_{fs}, T_{ms} and T_m (b) and SEM micrograph of the interface V10/preoxidised Crofer22APU after the joining treatment at 850°C for 1h in air.

The crystallization of the parent glass plays a fundamental role in the final properties of the sealing material. Fig.2 depicts the XRD diffraction patterns collected for the V10 glass-ceramic after different thermal treatments; the as-joined sample is shown in Fig.2a, while figures 2b an 2c present samples following aging at 800°C for 100h and 300h respectively. After the joining process, Al-containing diopside ($Ca(Mg,Al)(Si,Al)_2O_6$, PDF #00-041-1370) was identified as the main crystalline phase. The peaks of nepheline ($NaAlSiO_4$, PDF #00-035-0424) are also present in the patterns of both aged samples together with the peaks of diopside. The crystallization of nepheline during the initial stages of aging occurs adjacent to the diopside phase and separates the Na from Cr_2O_3. This could be beneficial

as the Na is “trapped” in the crystalline nepheline phase and thus limiting its potential to react with Cr as reported previously by Smeacetto et al. [47]. The results of Rietveld analyses are summarized in Table 1. Comparing Fig.2 with Table 1, it is noticeable that after aging at 800°C for 100 hrs, the amount of amorphous phase decreased in accordance with the crystallization of nepheline and the increase in the diopside content. However, the glass-ceramic system seems to be stable after this period, considering that after 300h of aging no new phases and no significant changes in the relative amounts of each phase were detected. This is very important, because a sealant should maintain a certain level of stability during the entire operating life of a SOC device, as excessive variations in the nature or amount of the crystalline phases could lead to detrimental changes in the thermo-mechanical properties of the sealant and maybe to sealant failure. Furthermore, the XRD quantitative analyses highlighted a significant amount of residual glassy phase which could be useful during thermal cycling giving rise to possible self-healing behaviour.

In order to study the evolution of the CTE of the material due to its partial crystallization, dilatometer measurements were carried out on the as-cast V10 glass and on the glass-ceramic after the joining process, as well as after aging for 100h and 300h at 800°C. The results are presented in Fig.3 together with the CTE values measured between 200°C and 500°C. The crystallization of diopside during the joining treatment increased the CTE of the material from 7.6 10^{-6} K^{-1} to 11.5 10^{-6} K^{-1} (both values were evaluated in the range 300-500°C). This is a reasonable result considering the CTE of the diopside (11.6 10^{-6} K^{-1}) [23]. The evolution of the crystalline phases during aging slightly affected the CTE value of the glass-ceramic lowering it to 11.2 10^{-6} K^{-1} (300-500°C) after 100h of aging at 800°C. This is due to the formation of around 8wt% of nepheline (Table 1) with a CTE of 9 10^{-6} K^{-1} [48], maybe partially counterbalanced by a further increase in the diopside content (from 37wt%

to 43wt%). The quantitative and qualitative stability in terms of crystalline phases previously discussed, is confirmed by the DIL measurements. Indeed, the CTE value (11.3 10^{-6} K-1) measured after aging for 300h does not differ significantly from the one recorded after aging for 100h. However, all the recorded values inherent to the glass-ceramic indicate very good thermo-mechanical compatibility with Crofer22APU stainless steel which has a CTE of 11.9 10^{-6} K^{-1} (between 25°C and 800°C) [49].

Furthermore, the amount of diopside contained in the glass-ceramic (Table 1) confirms the tailoring of the starting composition as intended by the authors. Indeed, the increased content of Ca in comparison with the previous system studied (labelled V9) [22] led to an effective increase in the content of this crystalline compound after aging. Thus, V10 contains around 5-6 wt% more diopside than V9. The main purpose of increasing the amount of diopside was to raise the CTE of the glass-ceramic to a value closer to that for Crofer22APU. This target has been successfully achieved; the CTE of V10 glass-ceramic after aging was 11.310^{-6} K^{-1} in comparison to the value of 9.6 10^{-6} $K^{-1}$for V9.

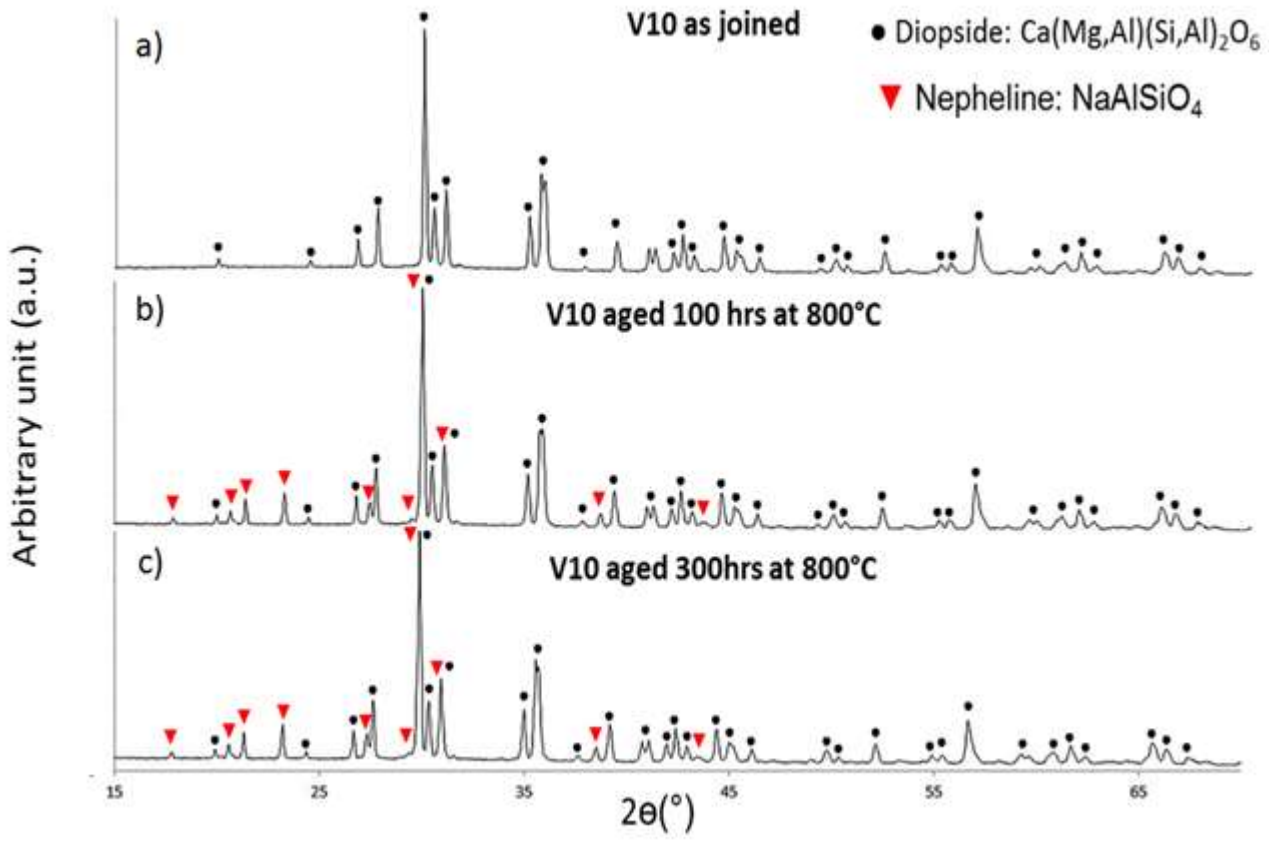

Figure2: XRD indexed patterns of V10 glass-ceramic after the joining process (a), after an aging at 800°C for 100h (b) and for 300h (c).

Table 1: Quantitative results of Rietveld refinement method on V10 glass-ceramic afterthe joining process, after an aging at 800°C for 100h and 300h.

Wt%	Amorphous	Diopside $Ca(Mg,Al)(Si,Al)_2O_6$	Nepheline $NaAlSiO_4$
As-joined	63	37	-
Aged 100h	49	43	8
Aged 300h	50	42	8

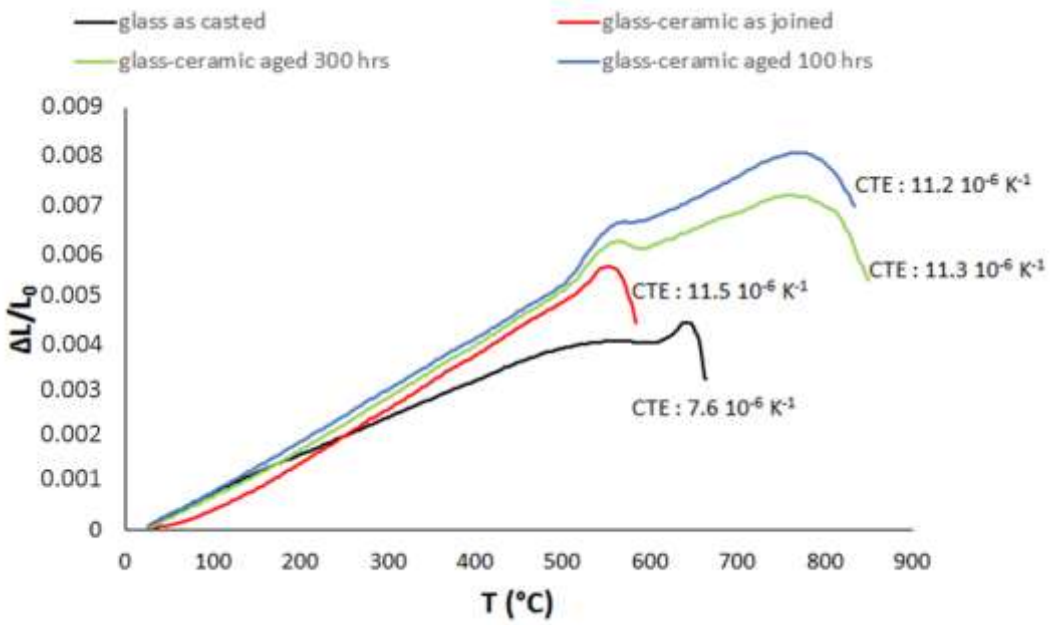

Figure 3: DIL measurements for V10 glass as-casted, after the joining thermal treatment and glass-ceramic after different aging periods at 800°C.

Crofer22APU/V10/Crofer22APUjoined samples were tested in dual atmosphere in the presence of 1.3Vand 0.7V applied voltage for 100h at 800°C. The results of electrical resistivity measurements are shown in Fig.4 together with electrical resistivity data for a reference V10 glass-ceramic sample that was not in contact with the Crofer22APU steel. These data were measured in air at 800°C for the same period. In Fig 4, the value of 10^4 Ω cm is marked with a dotted line. This value is considered the minimum below which current shunting might take place [12,13]. The V10 glass-ceramic maintained satisfactory values of resistivity for the entire test. During the first 20h of the test, a rapid increase in the electrical resistivity was measured; this could be due to the crystallization of nepheline during this period, trapping the Na^+ ions and reducing their mobility. Indeed, the alkali ions are widely considered to be charge carriers in glasses at temperatures higher than the T_g of the glass [35]. The sample to which 0.7V was applied exhibited a behaviour which is more similar to the one of the reference glass-ceramic for some aspects. The recorded values for this sample (0.7V) were in a range of 10^5-10^6 Ω cm, slightly lower than the

values corresponding to the reference glass-ceramic. However, the recorded values were stable and acceptable for the entire test. The sample that was subjected to an electrical potential of 1.3V, experienced a fast decrease in the resistivity. The electrical resistivity values were observed to be below the limit value (10^4 Ω cm) required to avoid current shunting in SOC stacks, especially in case of SOEC operation.

Chou et al. [33-35] studied an alkali-containing compliant silicate glass (containing Na and K) and it was electrically tested in dual environment with plain, aluminized and YSZ-coated AISI441 substrates. They observed a strong reduction in the electrical resistivity of the samples produced with bare stainless steel. On the other hand, the joint obtained with the passivated steel maintained a desirable electrical resistivity. This behaviour was ascribed to two phenomena; (i) the mobility of free alkali ions in theglassy material above T_g (considered as charge carriers) and (ii) the diffusion of elements from the non-passivated steel into the sealant with consequent microstructural changes.

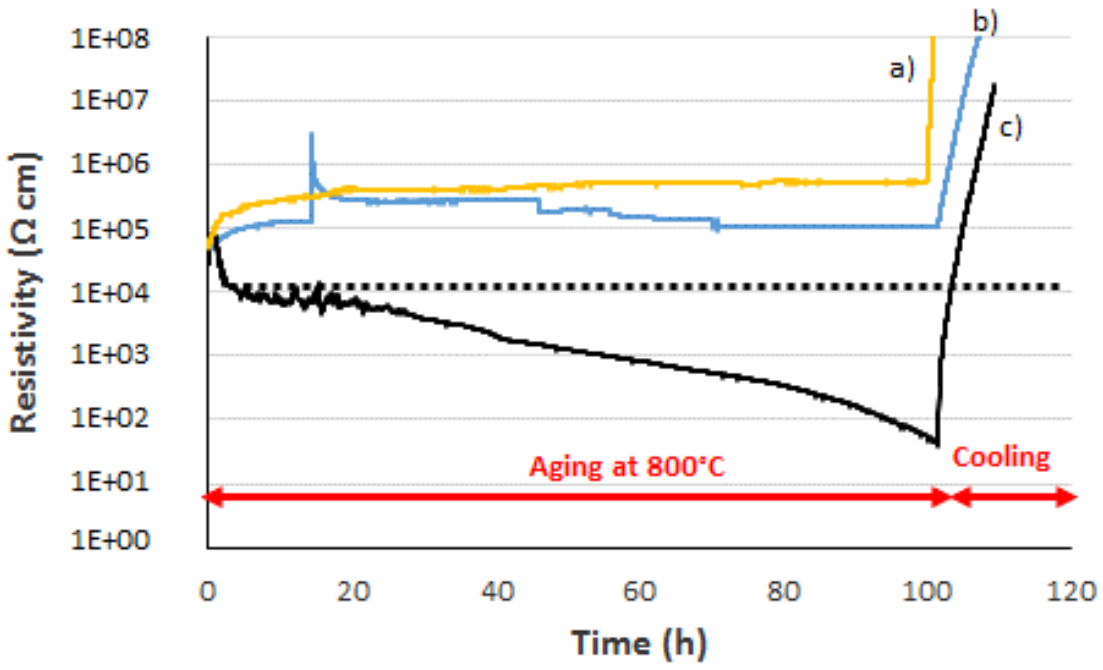

Figure 4: Resistivity values at 800°C for 100 h of the glass-ceramic itself with 1.3V applied voltage (a) and the joints exposed to dual atm. with both 0.7V (b) and 1.3V (c).

Post mortem SEM/EDS cross-section analyses of Crofer22APU/V10/Crofer22APU joints in the middle part of the joining are shown in Fig. 5 (application of 0.7V) and Fig. 6 (application of 1.3V) respectively. The two polarised interfaces differ significantly from each other. At the anodically (positive) polarised interface with 0.7V applied (Fig. 5a) no Cr diffusion was detected into the glass-ceramic, as evidenced by the EDS analysis at point 2; EDS analysis at point 1 confirmed the presence of nepheline as the minor crystalline phase, while elongated crystals, preferentially nucleating and growing from the MnCr-oxide layers, represent the main diopside crystalline phase. The examination at the cathodic (negative) polarised interface (Fig. 5b) revealed Mg-Mn-Cr rich crystals (point 4), together with Cr presence in the glassy phase of the glass-ceramic sealant (point3).

The application of a higher voltage (1.3V) led to significant differences such as the formation of Cr rich regions (EDS point 3) in the proximity of pores in the glass-ceramic sealant, as indicated by the red arrows in Fig. 6b. The development of these CrO_x regions was unlikely to be due to Cr diffusion from the cathodic polarised interface (see EDS point 3); the presence of substantial amounts of Cr (around 35 at%) within the porous areas is likely to have taken place due to volatilization. This conclusion was drawn because the concentration of Cr moving away from the interface with the pre-oxidised Crofer22APU was only 4at% (EDS point 2), while within porous areas further away the amount of Cr reached 35 at%. The low concentration of Cr close to the interface was due to diffusion, while the high concentration further away was due to vaporization and condensation. The morphology of CrO_x grown in the pores also suggests the condensation of a volatile compound.

The outward diffusion of Cr, from the cathodically polarised steel plates for both 0.7V and 1.3V applied voltage, led to the formation of pores beneath the oxide scale on the surface of the Crofer22APU. At this interface, the oxide scale appears to be irregular and thinner

than in the case of the anodically polarised interface, where oxides seem to be grown in the steel just below the scale (Fig. 6b). However, the glass-ceramic remained well-bonded onto the steel at both interfaces.

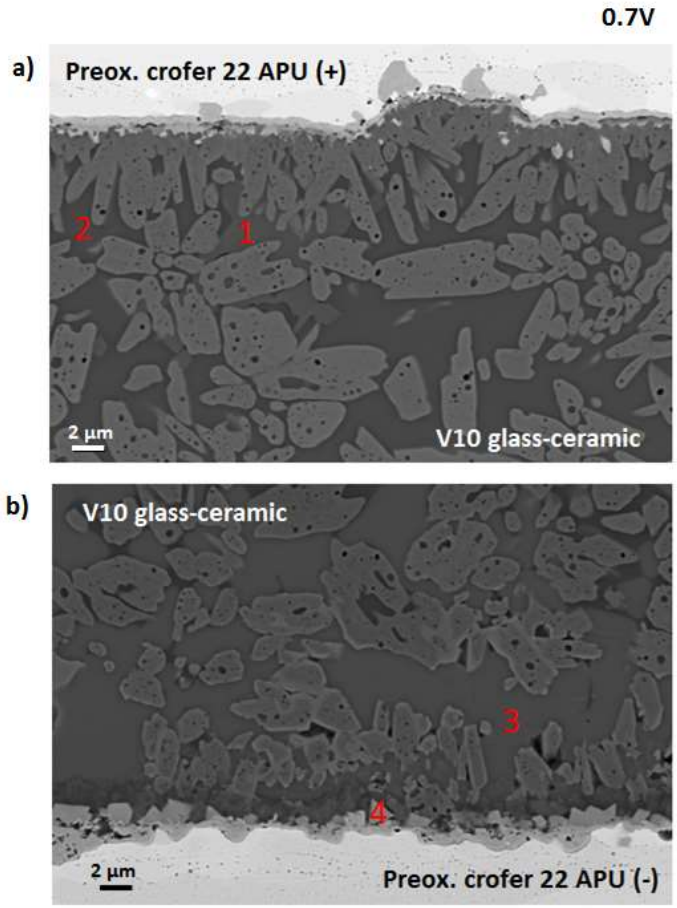

1

At%	
O	64.8
Na	8.7
Mg	1
Al	8.3
Si	16.5
Ca	0.4
Cr	0.1
Fe	0.2

2

At %	
O	61.3
Na	10.3
Mg	0.8
Al	10.6
Si	16.5
Ca	0.5

3

At%	
O	59.1
Na	5.8
Mg	1.5
Al	6.9
Si	18.6
Ca	3.4
Cr	4.6
Mn	0.1

4

At%	
O	65.2
Na	0.4
Mg	9.3
Al	0.5
Si	0.9
Ca	0.1
Cr	15
Mn	3.6
Fe	5

Figure 5: SEM/EDS analyses on the sample subjected to 0.7V: anodically (positive) polarized interface (a) andcathodically (negative) polarized one (b). The results of EDS carried out on the regions, marked with the red numbers, are reported in the corresponding tables.

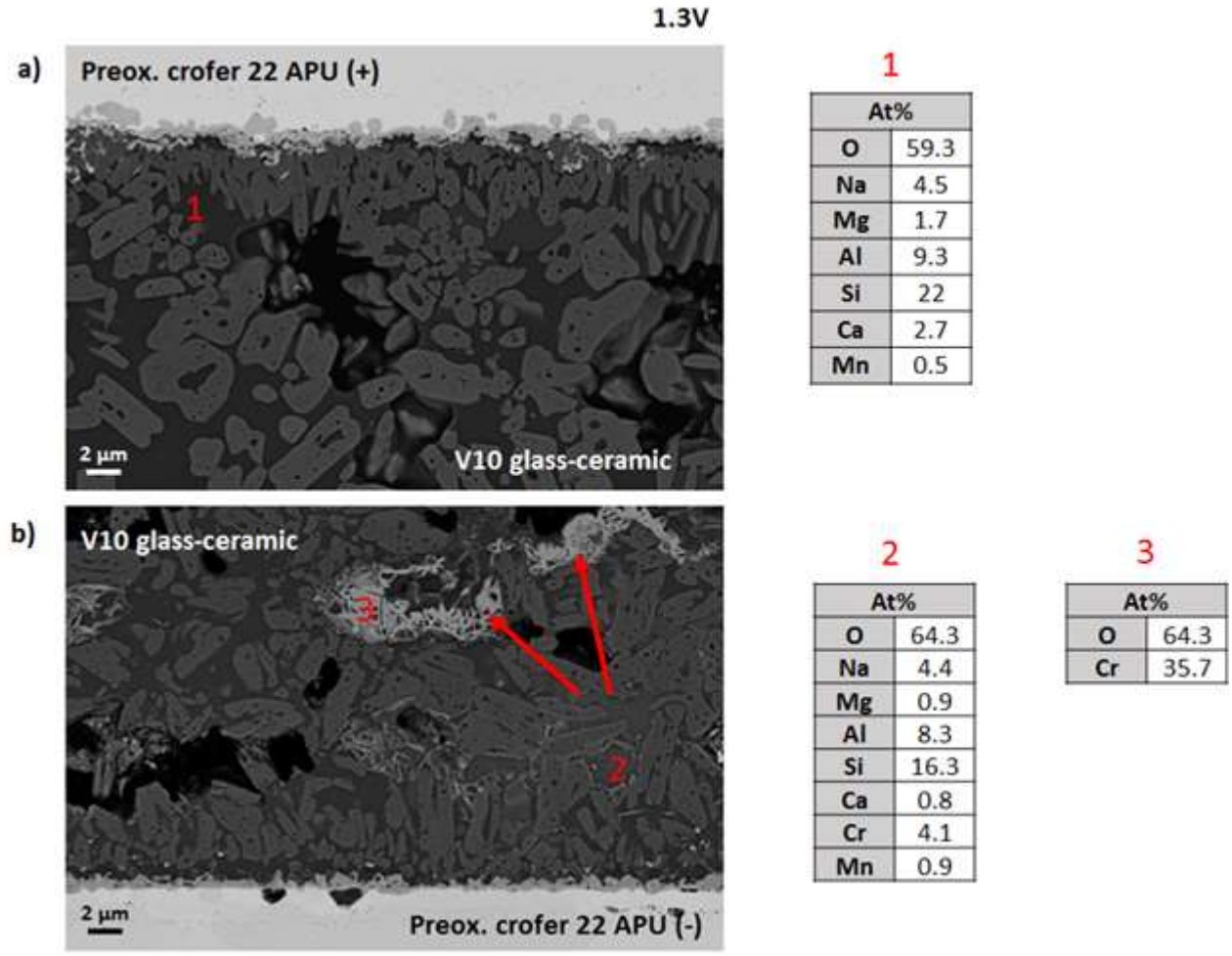

1	At%
O	59.3
Na	4.5
Mg	1.7
Al	9.3
Si	22
Ca	2.7
Mn	0.5

2	At%
O	64.3
Na	4.4
Mg	0.9
Al	8.3
Si	16.3
Ca	0.8
Cr	4.1
Mn	0.9

3	At%
O	64.3
Cr	35.7

Figure 6: SEM/EDS analyses of the sample subjected to 1.3V: anodically (positive) polarized interface (a) and cathodically (negative) polarized one (b). The results of EDS carried out on the regions, marked with the red numbers, are reported in the corresponding tables.

SEM micrographs collected at the air side of the joining subjected to 1.3V with static air are presented in Fig. 7 together with the results of EDS mapping. The white numbers in the picture correspond to the regionsat which EDS semi-quantitative point analyses were carried out. These results are summarized in Table2.

The external part of the sealant in contact with air appears to have degraded during the test. In spite of this, the joint remained sound; this was confirmed by further analyses (not reported here) carried out within the middle of the sample as well as close tothe reducing side. Furthermore, the results of leakage tests showed that leakage rates of these samples

lay between 10^{-11} and 10^{-10} mbar l s^{-1}, thus confirming gas tightness of the joints after the test.

The most interesting observation is the evidence of formation of a bright (in SEM backscattered mode) compound which grew starting from the negative polarized plate. The EDS maps revealed the presence of Cr and O. EDS point analyses (marked as point 1 in the SEM micrograph) were also collected in this region leading to a composition of: 45.1at% of Cr and 54.9at% of O. This suggests that this compound consists of chromia (Cr_2O_3).

The observed decrease of the electrical resistivity in Fig. 4 could be attributed to the formation of these products which provided a bridging effect between the two Crofer22APU plates, thus lowering the measured resistivity. Indeed, at 800°C the chromia has an electrical resistivity much lower than the V10 glass-ceramic (lower than ≈10^2 Ω cm) [50,51].

In the anodic polarized steel, a region rich in Fe and O but poor in Cr was formed during the test (marked in red in Fig. 7), suggesting the development of breakaway corrosion. Immediately below this region, Mg, O and Fe were detected together with minor amounts of Si, Al, Ca and Na (marked as point 3). This may suggest that the sealant was present there at the beginning of the test and then degraded. The presence of Fe is due to outward diffusion of this element from the steel, in accordance with the breakaway corrosion. Furthermore, the oxide scale at the anodic side appears to be very thick (≈20μm). The EDS results collected at point 4 (reported in Table 2) show that this scale was rich in Fe whose amount was greater thanfor Cr. This means that there was a non-protective effect by the scale grown during the test. A lack of Cr may be the reason of this phenomenon. In addition, the positive polarization of the plate may further enhance the oxidation of the

steel leading to its corrosion in the absence of the conventional protective layer formed by Crofer22APU and composed of Cr_2O_3 and $(Mn,Cr)_3O_4$.

In Fig.8, an SEM micrograph from an area close to the air side of the sample subjected to 0.7V is presented. It was apparent that there was no chromia “bridge” in this sample. Therefore, the formation of the “bridge” seems to be dependenton the applied voltage and was observed only in the samples that were exposed to the higher voltage (1.3V). Furthermore, the sealant appears to be intact, without any degradation effects during aging of the sample, as shown in Fig.8.

Therefore, the degradation phenomena seem to be the result from an interaction between the glass-ceramic sealant and the steel plates in presence of the higher applied voltage (1.3V). Cr-forming alloys are well known to develop Cr-containing volatile species in the typical SOFC operating conditions [52,53]. In particular, the main volatile product due to Cr vaporization is $CrO_2(OH)_2$, even in relatively dry oxidising atmosphere following the reaction [52,53]:

$$Cr_2O_{3(s)} + 2H_2O_{(g)} + 3/2O_{2(g)} \leftrightarrow 2CrO_2(OH)_{2(g)} \qquad \text{eq.1}$$

When alkali metals (denoted as R) are contained in the glass-ceramic sealants, such as Na in the present case, there can be some additional compounds due to reaction between $CrO_2(OH)_2$ and R_2O or ROH and between Cr_2O_3, O_2 and ROH. These reaction mechanisms have already been discussed by Ingram et al. [54] with respect to the behaviour of potassium in SOFC environments. From their results, eq. 2 can be adopted for the alkali metal sodium:

$$Cr_2O_{3(s)} + 4NaOH_{(g)} + 3/2\ O_{2(g)} + 2H_2O_{(g)} \leftrightarrow 2Na_2CrO_{4(g)} + 4H_2O_{(g)} \qquad \text{eq.2}$$

In order to estimate the driving force of the reaction, the free enthalpy and the Nernst potential for eq. 2 were calculated using FactSage® software. For our estimation we have

considered $NaCr_2O_4$ as a solid phase. At temperature of 800°C the calculation resulted in a free reaction enthalpy (ΔG^0) of -688,9 kJ/mol and a Nernst potential of 1,19V including 6 electrons involved in the redox reaction.

Eq. 2 represents a sum of several individual reactions, which can take place one after the other or in parallel. In eq. 2 two species Cr ($2Cr^{3+} \leftrightarrow 2Cr^{6+} + 6e^-$, electrons produced) and O ($3/2\ O_2 + 6e^- \leftrightarrow 3O^{2-}$, electrons consumed) change their oxidation state. The total reaction in eq. 2 can be also considered as product of consequential reaction steps (eq. 1 and eq. 3):

$$2\ CrO_2(OH)_{2(g)} + 4\ NaOH_{(g)} \leftrightarrow Na_2CrO_{4(g)} + 4\ H_2O_{(g)} \qquad \text{eq. 3}$$

Where $CrO_2(OH)_{2(g)}$ is produced from eq.1. Furthermore, a much higher amount of sodium is present on the surface of the solid glass ceramic sealant. Therefore, also the reaction where $Na_2O_{(s)}$ denotes the sodium dissolved in the glassy phase or contained in the crystalline phase nepheline should be possible instead of or in parallel to eq. 3:

$$CrO_2(OH)_{2(g)} + Na_2O_{(s)} \leftrightarrow Na_2CrO_{4(g)} + H_2O_{(g)} \text{eq. 4}$$

All the previous reactions have Na_2CrO_4 as product, which is highly volatile at 800°C and has a partial pressure much higher than $CrO_2(OH)_2$. The same was reported in the case of K_2CrO_4 by Ingram et al. [54]. This means that in case of eq. 2 and eq.4 a much higher Cr depletion from the steel is expected than in case of eq.1. A higher Cr-depletion leads to a non-protective oxide scale on the surface of the steel causing the corrosion and diffusion phenomena highlighted while discussing Fig. 7. Indeed, the reaction of $CrO_2(OH)_2$ will move the equilibrium of eq. 1 on the right preventing the system to reach an equilibrium state and leading to a continuous depletion of Cr from the steel.

On the one hand the results of the thermodynamic calculation of eq. 2 by FactSage® have shown clearly, that the oxidation of Cr_2O_3 in presence of oxygen has a strongly negative

ΔG and is therefore possible at 800°C. On the other hand, our SEM and EDX-results have clearly detected a Cr_2O_3 bridge and dendrites which bridged the two steel substrates (fig 7). It can be excluded that the layer and the dendrites consist of a hexavalent chromium oxide, since CrO_3 decomposes above 200°C into Cr_2O_3 and O_2. Hence it can be supposed that the formation of Cr_2O_3 is somewhat forced by an electrochemical potential which has a reducing effect. This situation is given by the cathodic polarization of one steel substrate effected by the applied potentials of 0,7V and 1,3V. If we assume that the gaseous Na_2CrO_4 species serve as a chromium source for the Cr_2O_3-bridge, the following reaction mechanism can be proposed. In a first step the gaseous Na_2CrO_4 species condensates on the surface of the cathodically polarized steel substrate ($Na_2CrO_{4(g)} \rightarrow Na_2CrO_{4(s)}$). Caused by the cathodic polarization of the steel substrate there exists a shifted electrochemical potential, which enables the decomposition of Na_2CrO_4 according to eq. 5, and due to the good electrical conductivity of the formed Cr_2O_3-scale the reaction can proceed easily.

$$2Na_2CrO_{4(s)} + 2H_2O_{(g)} \rightarrow Cr_2O_{3(s)} + 3/2\ O_2 + 4NaOH_{(g)} \quad \text{eq.5}$$

In fact, eq. 5 is the reverse reaction of eq.2 and by taking into account that the reaction has a nominal Nernst-Potential of 1,19 V at 800 °C it can be understood, that the formation of the Cr_2O_3-bridge is observed when potential of 1,3 V is applied. A potential of 0,7 V is not high enough in order to enable the reversal reaction according eq.5.

The NaOH, produced in the previous reaction, could react again with $CrO_2(OH)_2$ or with Cr_2O_3 close to the anodic plate to form again Na_2CrO_4 (eq.2 and 4). A similar mechanism is expected at the cathode of a hypothetic cell. The interaction of Na with Cr at high applied potentials can lead to a fast degradation of the cathode in case of sealing between the cells and metallic frames/interconnects or to a high current shunting in case of sealing between the metallic frame and interconnect plates or between two interconnect plates (as simulated in the present work). Furthermore, the presence of Na in the sealant represents

a continuous source of this element for the evaporation of Cr and a driving force for the degradation phenomena highlighted here.

As discussed, the application of the voltage plays a fundamental role in these mechanisms otherwise similar degradation phenomena would be observed in the case of 0.7V applied voltage. An electrical load higher than a threshold (between 0.7V and 1.3V) pushed the oxidation reactions of Cr at the anodically polarized interface with formation of volatile Cr-containing species and its reduction at the cathodically polarized one; thus leading to the formation of the Cr_2O_3 “bridges”, to a fast corrosion of the anodically polarized interconnect and to a fast degradation of the sealant close to the air side (Fig. 7).The higher applied voltage did not influence only the condensation of Cr_2O_3 at the cathodically polarized plate, but also promoted eq.1 and 2, otherwise corrosion phenomena and sealant degradation would be expected also in the sample to which 0.7V were applied.

The evidence from this study suggests that the presence of Na in the glass-ceramic is not enough to activate these evaporation and condensation reactions. Indeed, the degradation phenomena were detected only when the higher voltage (1.3V) was applied during the test. A possible solution to avoid the degradation described here might involve the deposition on the steel of protective coatings such as Al_2O_3 or YSZ. Indeed, as reported previously by Chou et al. [33-35], an alkali containing sealant in contact with coated Cr-containing steel did not show degradation in the resistivity, thus indicating a limitation in the formation of Na_2CrO_4 and its reduction to Cr_2O_3 in absence of interconnect surface as Chromium source.

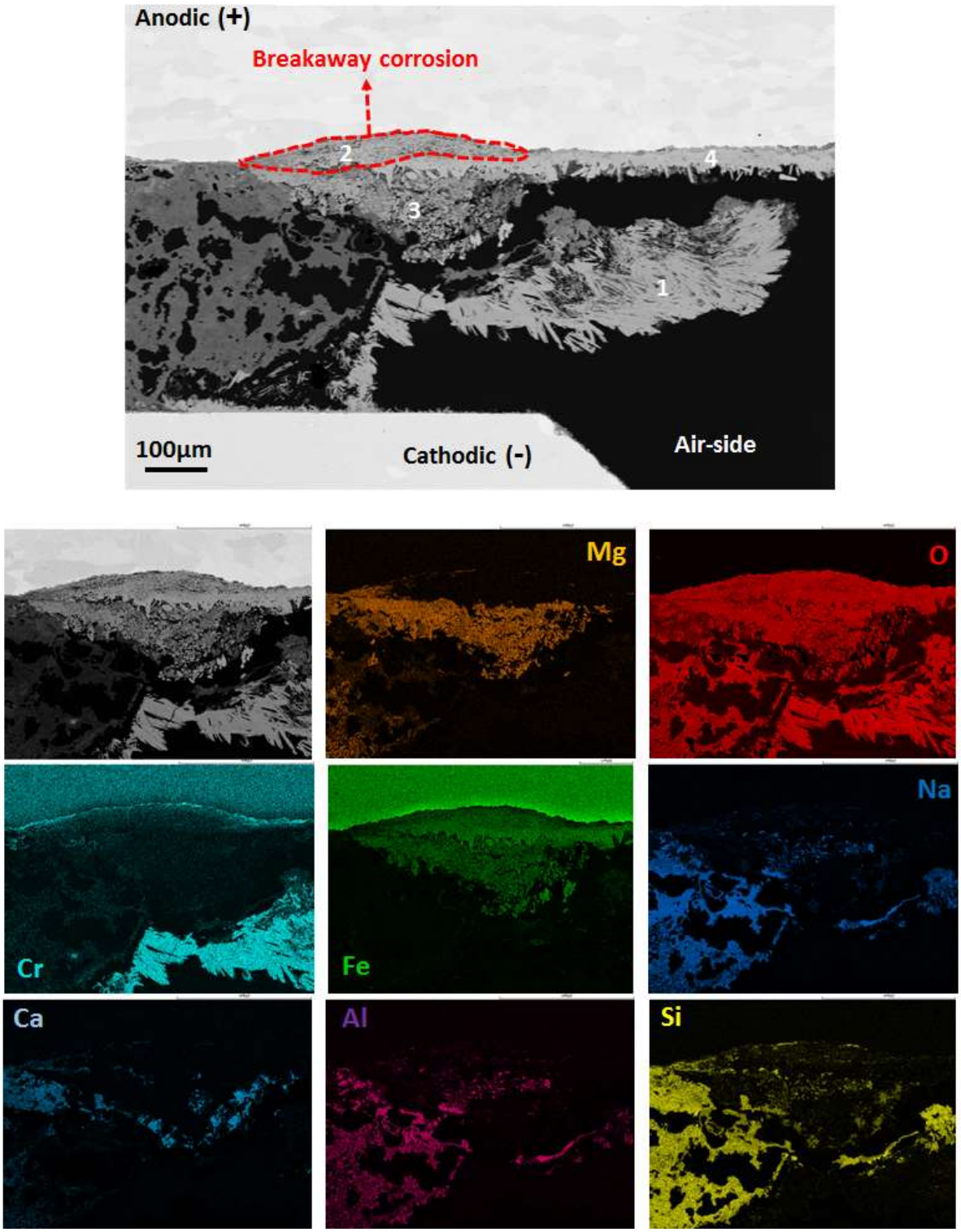

Figure 7: SEM and EDS maps collected at the air side of the sample subjected to dual atm. test for 100h at 800°C with 1.6V applied voltage.

Table 2: semi-quantitative EDS point analysis results collected on the points marked in Fig. 7.

	EDS Points			
Elements (at%)	1	2	3	4
Cr	45.1	4.6	0.8	3.4
O	54.9	63	62	60.3
Fe	-	28.7	23.5	36.3
Mg	-	0.1	9.1	-
Si	-	2	0.9	-
Al	-	0.4	0.5	-
Ca	-	0.2	1.7	-
Na	-	1	0.7	-
Mn	-	-	0.8	-

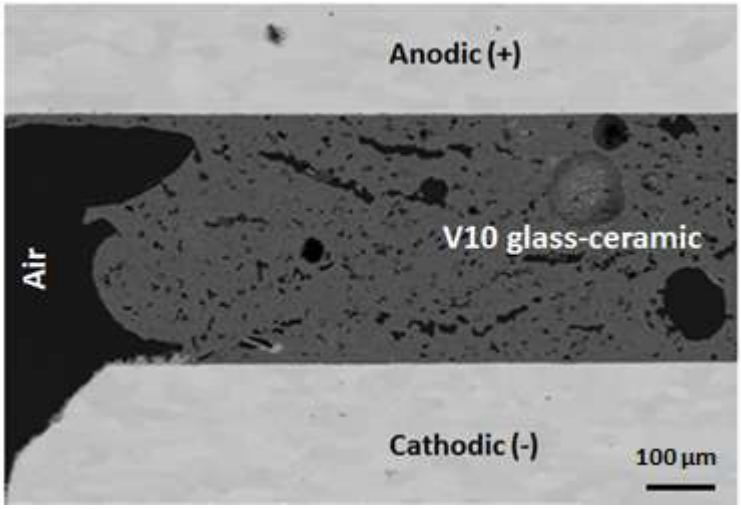

Figure 8:SEM micrographs of the sample Crofer22APU/V10/Crofer22APU subjected to dual atm. test at 800°C: for 100h with 0.7V applied voltage.

Conclusions

A new Na-containing diopside-based glass ceramic sealant composition was designed to match the CTE of the Crofer22APU interconnect. The sealant showed optimal properties in terms of sinter-crystallization behaviour (no overlap between sintering and crystallization) and CTE (11.3 10^{-6} K^{-1}). Diopside was detected as the main crystalline phase after both the joining treatment as well as after different aging periods. Nepheline was also detected as a secondary phase after aging of the glass-ceramic. The sealant composition promoted heterogeneous nucleation of diopside at the interface with the interconnect and provided a barrier between sodium and Cr_2O_3. Resistivity measurements

were carried out at 800°C for 100h. The results of these tests showed a suitable resistivity value for the glass-ceramic subjected to 1.3V (slightly lower than 10^6 Ω cm) and for the Crofer22APU/V10/Crofer22APU joined sample subjected to 0.7V and exposed to dual atmosphere (10^5-10^6 Ω cm). Significant degradation in the resistivity trend was recorded for the Crofer22APU/V10/Crofer22APU joined sample with 1.3V applied. This effect was due to the growth of Cr_2O_3 starting from the anodically polarized interface, which may have put in contact the two steel plates, lowering the overall measured resistivity. Together with the formation of this compound, in the same sample, breakaway corrosion and the degradation of the sealant were detected. The degradation of sealant resistance and interconnect corrosion at higher voltage can be explained by presence of Na_2CrO_4 which is volatile at 800°C and can overtake Chromium transport from anodically polarized interface to cathodically polarized one. At cathodically polarized interface Na_2CrO_4 can be decomposed applying anodic potential >1.19 V resulting in Cr_2O_3 which can grow from cathodically polarized side into glass forming Cr_2O_3 bridges decreasing glass isolation resistance. Furthermore, the absence of corrosion or sealant degradation in the sample subjected to 0.7V suggests that the applied voltage plays a role also in the vaporization of Cr-containing species from the steel and not only to their condensation to the catholically polarized plate.

The findings of this research provide insights for the use of Na-containing sealants when high applied voltage is used. The conclusions that can be drawn from the present study strengthen the idea that the use of a protective coating on the metallic interconnect will have a positive impact on the overall behaviour of the system minimizing observed corrosion phenomena, in presence of voltage in dual atmosphere.

References

[1] A. Choudhury, H. Chandra, A. Arora, Application of solid oxide fuel cell technology for power generation - A review, Renew. Sustain. Energy Rev. 20 (2013) 430–442. doi:10.1016/j.rser.2012.11.031.

[2] T. Elmer, M. Worall, S. Wu, S.B. Riffat, Fuel cell technology for domestic built environment applications: State of-the-art review, Renew. Sustain. Energy Rev. 42 (2015) 913–931. doi:10.1016/j.rser.2014.10.080.

[3] N.Q. Minh, Solid oxide fuel cell technology - Features and applications, Solid State Ionics. 174 (2004) 271–277. doi:10.1016/j.ssi.2004.07.042.

[4] O.Z. Sharaf, M.F. Orhan, An overview of fuel cell technology: Fundamentals and applications, Renew. Sustain. Energy Rev. 32 (2014) 810–853. doi:10.1016/j.rser.2014.01.012.

[5] S.C. Singhal, Solid oxide fuel cells for stationary, mobile, and military applications, Solid State Ionics. 152–153 (2002) 405–410. doi:10.1016/S0167-2738(02)00349-1.

[6] S.C. Singhal, K. Kendall, High-temperature solid oxide fuel cells: fundamentals, design, and applicatons, Elsevier Ltd., Oxford, 2003.

[7] P. Singh, N.Q. Minh, Solid Oxide Fuel Cells: Technology Status, Int. J. Appl. Ceram. Technol. 1 (2004) 5–15. doi:10.1111/j.1744-7402.2004.tb00149.x.

[8] V.N. Nguyen, L. Blum, Reversible fuel cells,Compehendium of Hydrogen Energy, Volume 3: Hydrogen Energy Conversion, Elsevier Ltd., 2016. doi:10.1016/B978-1-78242-363-8.00005-0.

[9] S.Y. Gómez, D. Hotza, Current developments in reversible solid oxide fuel cells, Renew. Sustain. Energy Rev. 61 (2016) 155–174. doi:10.1016/j.rser.2016.03.005.

[10] B. Timurkutluk, C. Timurkutluk, M.D. Mat, Y. Kaplan, A review on cell/stack designs for high performance solid oxide fuel cells, Renew. Sustain. Energy Rev. 56 (2016) 1101–1121. doi:10.1016/j.rser.2015.12.034.

[11] N. Mahato, A. Banerjee, A. Gupta, S. Omar, K. Balani, Progress in material selection for solid oxide fuel cell technology: A review, Prog. Mater. Sci. 72 (2015) 141–337. doi:10.1016/j.pmatsci.2015.01.001.

[12] M.K. Mahapatra, K. Lu, Glass-based seals for solid oxide fuel and electrolyzer cells - A review, Mater. Sci. Eng. R Reports. 67 (2010) 65–85. doi:10.1016/j.mser.2009.12.002.

[13] M.K. Mahapatra, K. Lu, Seal glass for solid oxide fuel cells, J. Power Sources. 195 (2010) 7129–7139. doi:10.1016/j.jpowsour.2010.06.003.

[14] D.U. Tulyaganov, A.A. Reddy, V. V. Kharton, J.M.F. Ferreira, Aluminosilicate-based sealants for SOFCs and other electrochemical applications - A brief review, J. Power Sources. 242 (2013) 486–502. doi:10.1016/j.jpowsour.2013.05.099 Review.

[15] S.-F. Wang, H.-C. Lu, Y.-X. Liu, Y.-F. Hsu, Z.-Y. Liu, Characteristics of glass sealants for intermediate-temperature solid oxide fuel cell applications, Ceram. Int. 43 (2017) 0–1. doi:10.1016/j.ceramint.2017.05.211.

[16] Y.S. Chou, J.W. Stevenson, G.G. Xia, Z.G. Yang, Electrical stability of a novel sealing glass with (Mn,Co)-spinel coated Crofer22APU in a simulated SOFC dual environment, J. Power Sources. 195 (2010) 5666–5673. doi:10.1016/j.jpowsour.2010.03.052.

[17] A. Goel, D.U. Tulyaganov, V. V. Kharton, A.A. Yaremchenko, J.M.F. Ferreira, Electrical behavior of aluminosilicate glass-ceramic sealants and their interaction with metallic solid oxide fuel cell interconnects, J. Power Sources. 195 (2010) 522–526. doi:10.1016/j.jpowsour.2009.08.007.

[18] V.A.C. Haanappel, V. Shemet, S.M. Gross, T. Koppitz, N.H. Menzler, M. Zahid, W.J. Quadakkers, Behaviour of various glass-ceramic sealants with ferritic steels under simulated SOFC stack conditions, J. Power Sources. 150 (2005) 86–100. doi:10.1016/j.jpowsour.2005.02.015.

[19] A.A. Reddy, D.U. Tulyaganov, M.J. Pascual, V. V. Kharton, E. V. Tsipis, V.A. Kolotygin, J.M.F. Ferreira, Diopside-Ba disilicate glass-ceramic sealants for SOFCs: Enhanced adhesion and thermal stability by Sr for Ca substitution, Int. J. Hydrogen Energy. 38 (2013) 3073–3086. doi:10.1016/j.ijhydene.2012.12.074.

[20] F. Smeacetto, A. De Miranda, A. Chrysanthou, E. Bernardo, M. Secco, M. Bindi, M. Salvo, A.G. Sabato, M. Ferraris, Novel glass-ceramic composition as sealant for SOFCs, J. Am. Ceram. Soc. 97 (2014) 3835–3842. doi:10.1111/jace.13219.

[21] A.A. Reddy, D.U. Tulyaganov, A. Goel, M.J. Pascual, V. V. Kharton, E. V. Tsipis, J.M.F. Ferreira, Diopside - Mg orthosilicate and diopside - Ba disilicate glass-ceramics for sealing applications in SOFC: Sintering and chemical interactions studies, Int. J. Hydrogen Energy. 37 (2012) 12528–12539. doi:10.1016/j.ijhydene.2012.05.130.

[22] A.G. Sabato, G. Cempura, D. Montinaro, A. Chrysanthou, M. Salvo, E. Bernardo, M. Secco, F. Smeacetto, Glass-ceramic sealant for solid oxide fuel cells application: Characterization and performance in dual atmosphere, J. Power Sources. 328 (2016) 262–270. doi:10.1016/j.jpowsour.2016.08.010.

[23] Y. Fei, Mineral physics and crystallography: a handbook of physical constants, The American Geophysical Union,Washinton, 1995, 29-44, doi:10.1029/RF002.

[24] A.K. Varshneya, Fundamental of Inorganic Glasses, Society of Glass Techonology, 2006, ISBN 0 900682 51 5.

[25] F. Smeacetto, A. Chrysanthou, M. Salvo, Z. Zhang, M. Ferraris, Performance and testing of glass-ceramic sealant used to join anode-supported-electrolyte to Crofer22APU in planar solid oxide fuel cells, J. Power Sources 190 (2009) 402–407. doi:10.1016/j.jpowsour.2009.01.042.

[26] A. Rost, J. Schilm, M. Kusnezoff, A. Reinert, Influence of electrical load on the stability of glass sealings, ECS Trans. 25 (2009) 1509–1518. doi:10.1149/1.3205685.

[27] Z. Yang, G. Xia, K.D. Meinhardt, K.S. Weil, J.W. Stevenson, Z. Yang, G. Xia, K.D. Meinhardt, K. Scott, Chemical Stability of Glass Seal Interfaces in Intermediate Temperature Solid Oxide Fuel Cells, J. Mater. Eng. Perform. 13 (2004) 327–334. doi:10.1361/10599490419298.

[28] M. Salvo, V. Casalegno, S. Rizzo, F. Smeacetto, A. Ventrella, M. Ferraris,Glasses and glass- ceramics as brazingmaterials for high-temperature applications, Advances in Brazing Science, Technology and Applications, Elsevier, 2013, doi:10.1533/9780857096500.3.525.

[29] K.A. Nielsen, M. Solvang, S.B.L. Nielsen, A.R. Dinesen, D. Beeaff, P.H. Larsen, Glass composite seals for SOFC application, J. Eur. Ceram. Soc. 27 (2007) 1817–1822. doi:10.1016/j.jeurceramsoc.2006.05.046.

[30] K. Ogasawara, H. Kameda, Y. Matsuzaki, T. Sakurai, Chemical Stability of Ferritic Alloy Interconnect for SOFCs, J. Electrochem. Soc. (2007) 657–663. doi:10.1149/1.2735919.

[31] D. Coillot, O. Me, New viscous sealing glasses for electrochemical cells, Int. J. Hydrogen Energy 7 (2012) 5–12. doi:10.1016/j.ijhydene.2012.02.194.

[32] S.P. Jiang, L. Christiansen, B. Hughan, K. Foger, Effect of glass sealant materials on microstructure and performance of Sr-doped LaMnO3 cathodes, J. Mater. Sci. Lett. 20 (2001) 695–697. doi:10.1023/A:1010950722533.

[33] Y.S. Chou, J.P. Choi, J.W. Stevenson, Compliant alkali silicate sealing glass for solid oxide fuel cell applications: The effect of protective alumina coating on electrical stability in dual environment, Int. J. Hydrogen Energy. 37 (2012) 18372–18380. doi:10.1016/j.ijhydene.2012.08.084.

[34] Y. Chou, E.C. Thomsen, R.T. Williams, J. Choi, N.L. Canfield, J.F. Bonnett, J.W. Stevenson, A. Shyam, E. Lara-curzio, Compliant alkali silicate sealing glass for solid oxide fuel cell applications : Thermal cycle stability and chemical compatibility, J. Power Sources 196 (2011) 2709–2716. doi:10.1016/j.jpowsour.2010.11.020.

[35] Y. Chou, E.C. Thomsen, J. Choi, J.W. Stevenson, Compliant alkali silicate sealing glass for solid oxide fuel cell applications : The effect of protective YSZ coating on electrical stability in dual environment, J. Power Sources. 202 (2012) 149–156. doi:10.1016/j.jpowsour.2011.11.017.

[36] F. Smeacetto, A. Chrysanthou, M. Salvo, T. Moskalewicz, F.D.H. Bytner, Thermal cycling and ageing of a glass-ceramic sealant for planar SOFCs, Int. J. Hydrogen Energy 6 (2011) 1–9. doi:10.1016/j.ijhydene.2011.04.083.

[37] F. Smeacetto, M. Salvo, M. Ferraris, J. Cho, A.R. Boccaccini, Glass – ceramic seal to join Crofer 22 APU alloy to YSZ ceramic in planar SOFCs, J. Eur. Ceram. Soc. 28 (2008) 61–68. doi:10.1016/j.jeurceramsoc.2007.05.006.

[38] F. Smeacetto, M. Salvo, M. Ferraris, V. Casalegno, P. Asinari, A. Chrysanthou, Characterization and performance of glass – ceramic sealant to join metallic interconnects

to YSZ and anode-supported-electrolyte in planar SOFCs, J. Eur. Ceram. Soc. 28 (2008) 2521–2527. doi:10.1016/j.jeurceramsoc.2008.03.035.

[39] F. Smeacetto, M. Salvo, F.D.D.H. Bytner, P. Leone, M. Ferraris, New glass and glass – ceramic sealants for planar solid oxide fuel cells, J. Eur. Ceram. Soc. 30 (2010) 933–940. doi:10.1016/j.jeurceramsoc.2009.09.033.

[40] J.G. Larsen, P.H. Larsen, C. Bagger, High Temperature Sealing Material,United States Patent, US 6,828,263 B2,2004.

[41] J.G. Larse, C. Olsen, M.D. Jensen, Solid Oxide Fuel Cell Stack Having a Glass Sealing Material, United States Patent, US 8,163,436 B2, 2012.

[42] W. Surdoval, E. Lara-Curzio, J. Stevenson, J. Muth, B.L. Armstrong, A. Shyam, M.L. Trejo, Y. Wang, Y.S. Chou, T. Shultz, Engineered glass seal for solid-oxide fuel cells, United States Patent, US2015/0030963 A1, 2015.

[43] A. Shyam, R. Trejo, D. McClurg, A. Ladouceur, M. Kirkham, X. Song, J. Howe, E. Lara-Curzio, Microstructural evolution in two alkali multicomponent silicate glasses as a result of long-term exposure to solid oxide fuel cell environments, J. Mater. Sci. 48 (2013) 5880–5898. doi:10.1007/s10853-013-7384-8.

[44] A.G. Sabato, A. Chrysanthou, M. Salvo, G. Cempura, F. Smeacetto, Interface stability between bare, Mn–Co spinel coated AISI 441 stainless steel and a diopside-based glass-ceramic sealant, Int. J. Hydrogen Energy. 43 (2018) 1824–1834. doi:10.1016/j.ijhydene.2017.11.150.

[45] A. Rost, J. Schilm, M. Kusnezoff, A. Michaelis, Degradation of sealing glasses under electrical load, J. Ceram. Sci. Tech. 3 (2012) 69–80. doi:10.4416/JCST2012-00002.

[46] A. Rost, J. Schilm, J. Suffner, M. Kusnezoff, A. Michaelis, Development and Testing of Sealing Glasses for SOFCs based on CFY-Interconnects, in: 11th Eur. SOFC SOE Forum 2014, Lucerne Swithzerland.

[47] F. Smeacetto, M. Salvo, M. Santarelli, P. Leone, G.A. Ortigoza-Villalba, A. Lanzini, L.C. Ajitdoss, M. Ferraris, Performance of a glass-ceramic sealant in a SOFC short stack, Int. J. Hydrogen Energy. 38 (2013) 588–596. doi:10.1016/j.ijhydene.2012.07.025.

[48] W. Holland, G. Beall, Glass-ceramic technology, The American Ceramic Society, Westerville, 2002.

[49] VDM-Metals, VDM ® Crofer 22 APU, (2010).

[50] K. Wang, Y. Liu, J.W. Fergus, Interactions between SOFC interconnect coating materials and chromia, J. Am. Ceram. Soc. 94 (2011) 4490–4495. doi:10.1111/j.1551-2916.2011.04749.x.

[51] S. Fontana, S. Chevalier, G. Caboche, Metallic interconnects for solid oxide fuel cell: Effect of water vapour on oxidation resistance of differently coated alloys, J. Power Sources. 193 (2009) 136–145. doi:10.1016/j.jpowsour.2008.11.041.

[52] M. Stanislowski, E. Wessel, K. Hilpert, T. Markus, L. Singheiser, Chromium Vaporization from High-Temperature Alloys, J. Electrochem. Soc. 154 (2007) A295. doi:10.1149/1.2434690.

[53] E.J. Opila, D.L. Myers, N.S. Jacobson, I.M.B. Nielsen, D.F. Johnson, J.K. Olminsky, M.D. Allendor, Theoretical and experimental investigation of the thermochemistry of CrO2(OH)2(g), J. Phys. Chem. A. 111 (2007) 1971–1980. doi:10.1021/jp0647380.

[54] B.J. Ingram, T.A. Cruse, M. Krumpelt, Potassium-assisted chromium transport in solid oxide fuel cells, J. Electrochem. Soc. 154 (2007) B1200–B1205. doi:10.1149/1.2781117.